



**HAL**  
open science

## Vertical Eddy Fluxes in the Southern Ocean

Jan D. Zika, Julien Le Sommer, Carolina O. Dufour, Jean-Marc Molines,  
Bernard Barnier, Pierre Brasseur, Raphaël Dussin, Thierry Penduff, Daniele  
Iudicone, Andrew Lenton, et al.

► **To cite this version:**

Jan D. Zika, Julien Le Sommer, Carolina O. Dufour, Jean-Marc Molines, Bernard Barnier, et al..  
Vertical Eddy Fluxes in the Southern Ocean. *Journal of Physical Oceanography*, 2013, 43, pp.941-  
955. 10.1175/JPO-D-12-0178.1 . hal-00873342

**HAL Id: hal-00873342**

**<https://hal.science/hal-00873342>**

Submitted on 11 Jun 2021

**HAL** is a multi-disciplinary open access archive for the deposit and dissemination of scientific research documents, whether they are published or not. The documents may come from teaching and research institutions in France or abroad, or from public or private research centers.

L'archive ouverte pluridisciplinaire **HAL**, est destinée au dépôt et à la diffusion de documents scientifiques de niveau recherche, publiés ou non, émanant des établissements d'enseignement et de recherche français ou étrangers, des laboratoires publics ou privés.

## Article (refereed) – Published version

---

Zika, Jan D.; Le Sommer, Julien; Dufour, Carolina O.; Molines, Jean-Marc; Barnier, Bernard; Brasseur, Pierre; Dussin, Raphaël; Penduff, Thierry; Iudicone, Daniele; Lenton, Andrew; Madec, Gurvan; Mathiot, Pierre; Orr, James; Shuckburgh, Emily; Vivier, Frederic. 2013 Vertical Eddy Fluxes in the Southern Ocean. *Journal of Physical Oceanography*, 43 (5). 941-955. [10.1175/JPO-D-12-0178.1](https://doi.org/10.1175/JPO-D-12-0178.1)

This version available at <http://nora.nerc.ac.uk/502395/>

NERC has developed NORA to enable users to access research outputs wholly or partially funded by NERC. Copyright and other rights for material on this site are retained by the rights owners. Users should read the terms and conditions of use of this material at

<http://nora.nerc.ac.uk/policies.html#access>

© Copyright 2013 American Meteorological Society (AMS).  
Permission to use figures, tables, and brief excerpts from this work in scientific and educational works is hereby granted provided that the source is acknowledged. Any use of material in this work that is determined to be “fair use” under Section 107 of the U.S. Copyright Act September 2010 Page 2 or that satisfies the conditions specified in Section 108 of the U.S. Copyright Act (17 USC §108, as revised by P.L. 94-553) does not require the AMS’s permission. Republication, systematic reproduction, posting in electronic form, such as on a web site or in a searchable database, or other uses of this material, except as exempted by the above statement, requires written permission or a license from the AMS. Additional details are provided in the AMS Copyright Policy, available on the AMS Web site located at (<http://www.ametsoc.org/>) or from the AMS at 617-227-2425 or [copyrights@ametsoc.org](mailto:copyrights@ametsoc.org).

Contact NOC NORA team at  
[publications@noc.soton.ac.uk](mailto:publications@noc.soton.ac.uk)

## Vertical Eddy Fluxes in the Southern Ocean

JAN D. ZIKA,\* JULIEN LE SOMMER,<sup>+</sup> CAROLINA O. DUFOUR,<sup>#</sup> JEAN-MARC MOLINES,<sup>+</sup>  
 BERNARD BARNIER,<sup>+</sup> PIERRE BRASSEUR,<sup>+</sup> RAPHAËL DUSSIN,<sup>+</sup> THIERRY PENDUFF,<sup>+</sup>  
 DANIELE IUDICONE,<sup>@</sup> ANDREW LENTON,<sup>&</sup> GURVAN MADEC,\*\* PIERRE MATHIOT,<sup>++</sup>  
 JAMES ORR,<sup>##</sup> EMILY SHUCKBURGH,<sup>@@</sup> AND FREDERIC VIVIER<sup>&&</sup>

\* *Laboratoire des Ecoulements Geophysiques et Industriels, CNRS/Université de Grenoble, Grenoble, France, and  
 University of Southampton, National Oceanography Centre, Southampton, United Kingdom*

<sup>+</sup> *Laboratoire des Ecoulements Geophysiques et Industriels, CNRS/Université de Grenoble, Grenoble, France*

<sup>#</sup> *Laboratoire des Ecoulements Geophysiques et Industriels, CNRS/Université de Grenoble, Grenoble, and Laboratoire  
 des Sciences du Climat et l'Environnement, CEA-CNRS, Gif-sur-Yvette, France*

<sup>@</sup> *Stazione Zoologica Anton Dohrn, Naples, Italy*

<sup>&</sup> *CSIRO Marine and Atmospheric Research, Aspendale, Victoria, Australia*

\*\* *LOCEAN, UPMC/IPSL/IRD/CNRS, Paris, France, and NOCS, National Oceanographic Center,  
 Southampton, United Kingdom*

<sup>++</sup> *TECLIM, Earth and Life Institute, Louvain la Neuve, Belgium*

<sup>##</sup> *Laboratoire des Sciences du Climat et l'Environnement, CEA-CNRS, Gif-sur-Yvette, France*

<sup>@@</sup> *British Antarctic Survey, Cambridge, United Kingdom*

<sup>&&</sup> *LOCEAN, UPMC/IPSL/IRD/CNRS, Paris, France*

(Manuscript received 7 September 2012, in final form 28 November 2012)

### ABSTRACT

The overturning circulation of the Southern Ocean has been investigated using eddy-coupled ocean–sea ice models. The circulation is diagnosed in both density–latitude coordinates and in depth–density coordinates. Depth–density coordinates follow streamlines where the Antarctic Circumpolar Current is equivalent barotropic, capture the descent of Antarctic Bottom Water, follow density outcrops at the surface, and can be interpreted energetically. In density–latitude coordinates, wind-driven northward transport of light water and southward transport of dense water are compensated by standing meanders and to a lesser degree by transient eddies, consistent with previous results. In depth–density coordinates, however, wind-driven upwelling of dense water and downwelling of light water are compensated more strongly by transient eddy fluxes than fluxes because of standing meanders. Model realizations are discussed where the wind pattern of the southern annular mode is amplified. In density–latitude coordinates, meridional fluxes because of transient eddies can increase to counter changes in Ekman transport and decrease in response to changes in the standing meanders. In depth–density coordinates, vertical fluxes because of transient eddies directly counter changes in Ekman pumping.

### 1. Introduction

The Southern Ocean is a critical junction in the global oceanic circulation. The Southern Ocean overturning, in particular, exposes a substantial fraction of the deep ocean's water masses to the atmosphere and the Southern Ocean has contributed to around 40% of the oceanic uptake of anthropogenic CO<sub>2</sub> (Sabine et al. 2004). The precise dynamics of the Southern Ocean overturning are

thus critical to our understanding of the climate system and its sensitivity (see Rintoul et al. 2001, for a review of Southern Ocean dynamics).

Vigorous zonal winds over the Southern Ocean drive a northward Ekman transport of up to 30 Sv (1 Sv  $\equiv 10^6$  m<sup>3</sup> s<sup>-1</sup>). At latitudes of Drake Passage, the Southern Ocean is zonally unbounded. The northward Ekman transport cannot be balanced by a southward mean geostrophic flow, except below topography (around 2000-m depth). Thus, light surface waters are driven northward and downward north of Drake Passage and dense deep waters are driven southward and upward south of Drake Passage. Wind forcing manifests itself in the zonally averaged

*Corresponding author address:* Jan D. Zika, University of Southampton, National Oceanography Centre, SO14 3ZH, United Kingdom.

E-mail: j.d.zika@soton.ac.uk

overturning circulation as the “Deacon Cell” (Manabe et al. 1990).

It has been recognized that the Deacon Cell does not represent the exchanges of water masses in the Southern Ocean. This was most clearly demonstrated by Döös and Webb (1994). Using an eddy-permitting model, Döös and Webb (1994) diagnose the Southern Ocean circulation in density–latitude coordinates. They see no closed Deacon Cell but rather a small net northward transport of light water and southward transport of dense water on isopycnal layers.

Disagreement has arisen as to the process by which the wind-driven circulation is compensated. Döös and Webb (1994) argue that the northward transport of light water is compensated by standing meanders of the Antarctic Circumpolar Current (ACC). The ACC, they argue, transports light water southward in the open ocean and dense water northward along the coast of Argentina. Here we will use the general term “standing meanders” to describe contributions to the circulation from perturbations to the zonal mean, be they due to individual coherent recirculations or steady meanders of the ACC itself. In theoretical descriptions of the ACC, it is assumed that transient eddies act to flatten isopycnals, transporting light water southward and dense water northward across mean streamlines (Marshall and Radko 2003). We use the general term “transient eddy” to describe contributions due to all transient processes be they, for example, moving coherent vortices, turbulent fluctuations, or transient meandering of jets.

The circulation of fine-resolution models, diagnosed in density–latitude coordinates (Lee and Coward 2003; Hallberg and Gnanadesikan 2006), tend to reveal a “sub-polar” cell fluxing 5–10 Sv of dense water southward and light water northward. However, a complex series of additional overturning cells have been found, including a surface cell that constitutes a southward flux of light water and northward flux of dense water in the surface layers of the Southern Ocean (Lee and Coward 2003). Such cells neither conform to the theoretical descriptions of Marshall and Radko (2003) nor correspond with the circulation inferred from surface water mass transformation and observed tracer distributions such as those of Speer et al. (2000).

Lee and Coward (2003) and Treguier et al. (2007) diagnose the circulation of the Southern Ocean in density–streamline coordinates with streamlines defined by the time-mean depth-integrated streamfunction. They reveal an increased role of transient eddies in the upper cell of the Southern Ocean overturning. This suggests that, although the standing meanders compensate for the Deacon Cell meridionally, transient eddies still play a key role. In fact, Polton and Marshall (2007) have

shown that fluxes due to standing meanders vanish completely when following a streamline at constant depth defined by a Bernoulli potential.

Recently Nurser and Lee (2004) and Nycander et al. (2007) proposed diagnosing the oceanic circulation in depth–density coordinates. In such coordinates, net vertical exchanges of water masses are diagnosed by averaging the vertical velocity in density ranges at constant depth. Lee and Nurser (2012) have applied depth–density averaging to the circulation of an idealized channel model. Here we analyze the Southern Ocean overturning in state of the art eddying models of the Southern Ocean in both density–latitude coordinates and depth–density coordinates. Our results indicate that standing meanders and transient eddies play complementary, rather than independent roles, in compensating the wind-driven circulation of the Southern Ocean.

The simulations diagnosed in this study are described in section 2. Section 3 describes the overturning diagnostics that are applied to the models. In section 3c, we discuss a model simulation where the Southern Ocean winds have been increased. Advantages of depth–density coordinates and the evident limitations of the present suite of eddying models are discussed in section 4. Section 5 presents the key results of this study and implications for future work.

## 2. Coupled ocean–sea ice simulations

We analyze output of eddying model simulations performed with three configurations: PERIANT8, ORCA025, and PERIANT025. All are based on the coupled ocean–sea ice modeling framework: Nucleus for European Modeling of the Ocean (NEMO) version 3.1 (Madec 2008). In each configuration vertical mixing is represented with the turbulent kinetic energy closure scheme (order 1.5, Blanke and Delecluse 1993) with a background vertical mixing coefficient of  $5 \times 10^{-6} \text{ m}^2 \text{ s}^{-1}$  in PERIANT8 and  $1 \times 10^{-6} \text{ m}^2 \text{ s}^{-1}$  in ORCA025 and PERIANT025. There is no parameterization for eddy induced advection in any simulation discussed here.

Horizontal resolutions are  $1/8^\circ$  for PERIANT8 and  $1/4^\circ$  for ORCA025 and PERIANT025. Grid spacing scales with the cosine of latitude such that grid boxes are smaller at high latitudes (approximately  $6 \text{ km} \times 6 \text{ km}$  for PERIANT8 and  $13 \text{ km} \times 13 \text{ km}$  at  $60^\circ\text{S}$  for ORCA025 and PERIANT025). All models have 46 vertical levels.

ORCA025 is a global configuration described in detail in Barnier et al. (2006). The simulation discussed here is ORCA025-G70 (referred to as ORCA025 hereafter). It has been run over the period 1958–2004 with Drakkar Forcing Set 3 [DFS3, Brodeau et al. (2010), a composite of the 40-yr European Centre for Medium-Range

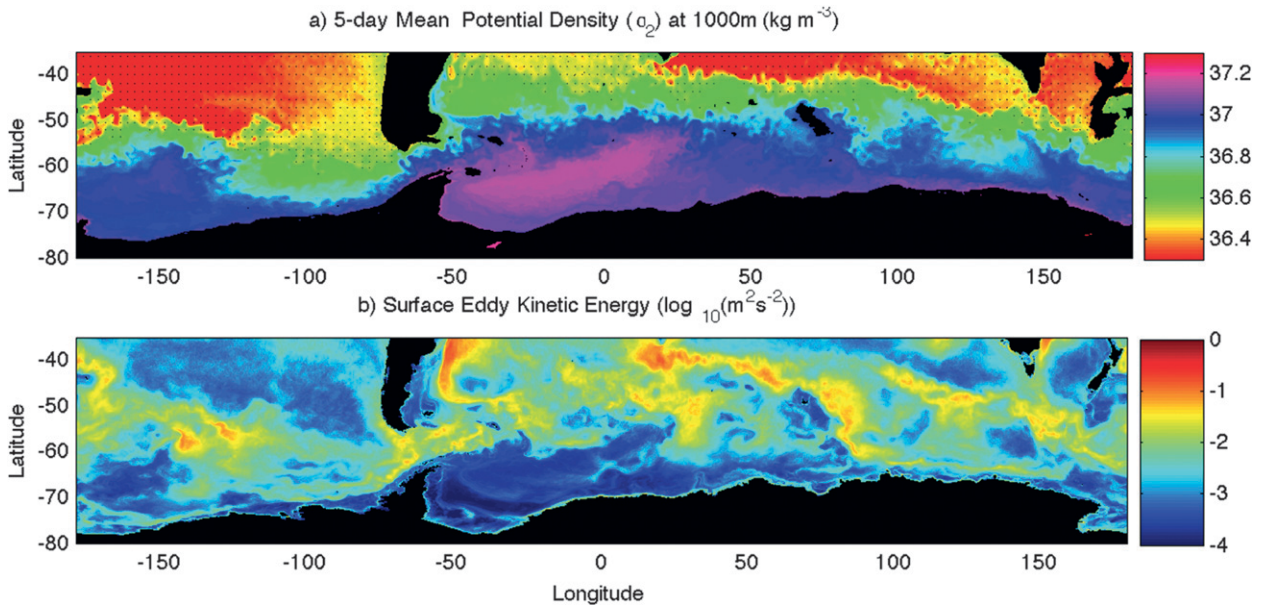


FIG. 1. (a) Potential density ( $\sigma_2$ ) at 1000-m depth for the final five-days of the PERIANT8 simulation (27–31 Dec 2007). Densities that straddle the northern boundary at this depth are dappled. (b)  $\log_{10}$  of mean eddy kinetic energy for the final 10 years (1998–2007) of the simulation.

Weather Forecasts (ECMWF) Re-Analysis (ERA-40) and ECMWF operational analyses and satellite products]. The simulation is discussed by Drakkar-Group (2007), has been investigated with respect to the Southern Ocean by Treguier et al. (2007), and has been thoroughly compared to altimeter observations in various frequency bands by Penduff et al. (2010).

PERIANT8 and PERIANT025 are regional model configurations representing all of the ocean south of 30°S. We will analyze the simulations PERIANT8-GJM01 (referred to as PERIANT8 hereafter) and two simulations of PERIANT025: PERIANT025-GCG3.1 (Here after PERIANT025-REF) and PERIANT025-GCWIND7 (Here after PERIANT025-SAM). The two PERIANT025 simulations were referred to as REF025 and SAM025+++ in Dufour et al. (2012). PERIANT025 is described in detail in Dufour et al. (2012). PERIANT8 is described for the first time here. Transport is permitted across the boundary at 30°S in the PERIANT simulations and temperature and salinity are restored to the output of ORCA025 using radiative boundary conditions there (Treguier et al. 2001).

PERIANT025 is forced at the sea surface using DFS3 over the period 1980–2004, while PERIANT8 is forced using the Drakkar Forcing Set 4 (Brodeau et al. 2010, DFS4 is based on ERA40 and ECMWF products and is essentially the same as DFS3 for the purposes of this study) over the period 1969–2007. An additional modification is made to the surface forcing in PERIANT8 that is not present in PERIANT025 or ORCA025. In PERIANT8 freshwater fluxes due to runoff and fixed

sea ice melt around Antarctica are distributed evenly over all the ocean within 100 km of the Antarctic Coast, rather than the closest coastal grid point as is done in ORCA025 and PERIANT025.

Treguier et al. (2007) have shown that sinking of dense water is not well represented in ORCA025. The consequent reduction in the total volume of Antarctic Bottom Water (AABW) around Antarctica leads to a strong trend in ACC transport (Treguier et al. 2007). In PERIANT8 and PERIANT025, to retain the volume of AABW, simulated temperature and salinity were restored to climatological values where  $\sigma_2 > 37.11 \text{ kg m}^{-3}$  (well below the sill depth at Drake Passage;  $\sigma_2$  is potential density referenced to 2000 m depth) with a restoring time scale of 2 yr. Experiments with PERIANT025 have demonstrated that this restoring substantially rectifies the decadal trend in ACC transport while not affecting variability of the flow on shorter time scales (Dufour et al. 2012). Surface salinity is also restored to climatological values in PERIANT8 and PERIANT025 with a piston velocity of 50 m (300 days)<sup>-1</sup>.

The ACC transport of PERIANT8, as measured at Drake Passage, rapidly adjusts during the first 5–10 yr of the model run from 150 Sv to around 125 Sv with interannual variability of  $\pm 5$  Sv. There is a small apparent trend of 2–3 Sv (decade)<sup>-1</sup>.

A five-day average of potential density at 1000-m depth in PERIANT8 shows the rich eddy field achieved (Fig. 1a). The signature of these eddies is evident in the surface eddy kinetic energy averaged over the final 10 years of the model simulation (1998–2007, Fig. 1b;

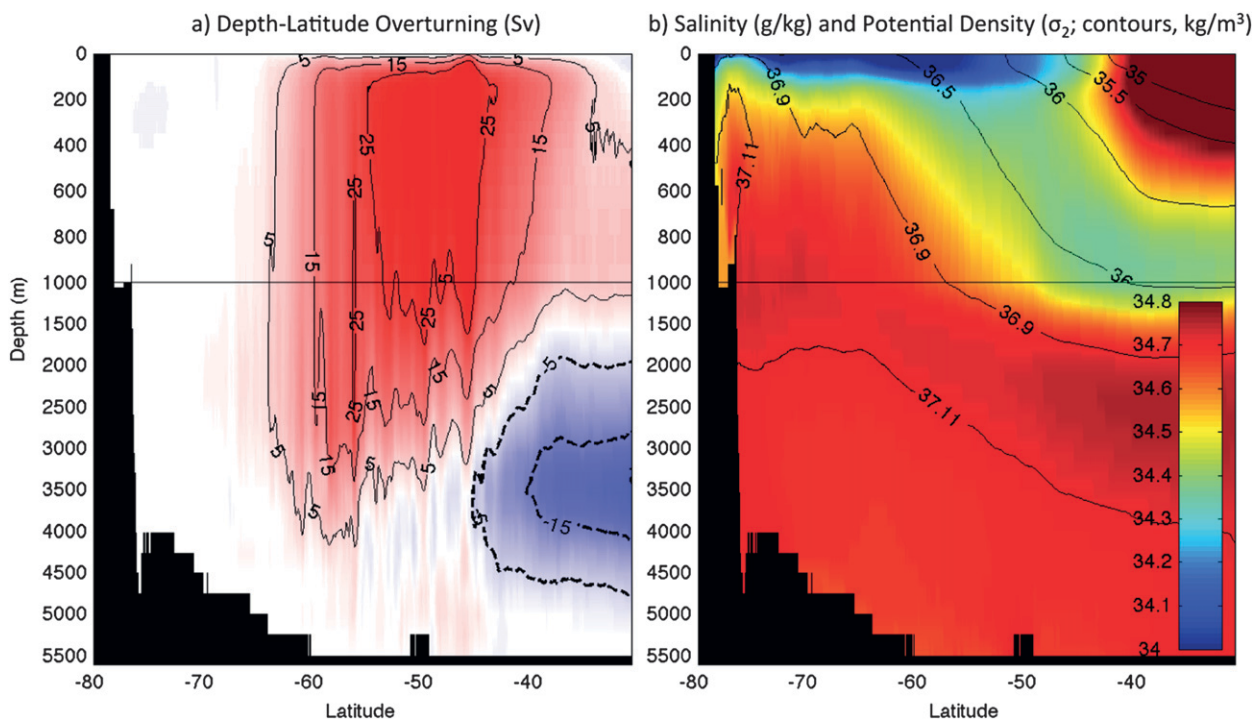


FIG. 2. (a) The overturning circulation of PERIANT8 averaged in depth-latitude coordinates ( $\Psi_{zy}$ ). Positive cells are clockwise (solid contours) and negative cells are anticlockwise (dashed contours). (b) Salinity (color;  $\text{g kg}^{-1}$ ) and potential density (contours;  $\sigma_2$ ,  $\text{kg m}^{-3}$ ) averaged at constant latitude and depth in PERIANT8.

$\text{EKE} = \overline{u'^2 + v'^2}/2$ ,  $u'$  and  $v'$  being the deviations from the annual mean surface zonal and meridional velocities respectively).

### 3. Overturning streamfunction diagnosis

Here we introduce various overturning diagnostics that will be used to diagnose different aspects of the circulation. Our first analysis of PERIANT8 focuses on the final 10 years of simulation (1998–2007). Analysis of ORCA025 will then be presented, including comparisons with a previous study by Treguier et al. (2007). Then we will analyze PERIANT025 and make comparisons with the recent study of Dufour et al. (2012).

#### a. PERIANT8 overturning

The depth–latitude overturning streamfunction  $\Psi_{zy}$  is defined as the temporal, zonal, and vertical integral of the meridional velocity

$$\Psi_{zy} = -\frac{1}{t_2 - t_1} \int_{t_1}^{t_2} \oint \int_0^z v(x, y, z^*, t) dz^* dx dt, \quad (1)$$

where  $z$  is depth,  $z^*$  is a dummy variable,  $y$  is latitude, and  $x$  is longitude. In PERIANT8,  $\Psi_{zy}$  reveals the wind-driven Deacon Cell (positive cell in Fig. 2a). A zonal

average of salinity and potential density (Fig. 2b), suggests that fluid parcels, which transport tracers in PERIANT8, do not follow  $\Psi_{zy}$  streamlines, but rather, closely follow isopycnal surfaces.

The density–latitude overturning streamfunction  $\Psi_{y\sigma}$  is defined as the temporal vertical and zonal integral of  $v$  over the area where  $\sigma_2^*$  is less than  $\sigma_2$ :

$$\Psi_{y\sigma} = -\frac{1}{t_2 - t_1} \int_{t_1}^{t_2} \oint \int_{\sigma_2^* \leq \sigma_2} v(x, y, z, t) dz dx dt. \quad (2)$$

We compute  $\Psi_{y\sigma}$  from five-day averages of PERIANT8 (Fig. 3a). The Deacon Cell, which is evident in the depth–latitude overturning, is no longer present in the density–latitude circulation. As in previous eddy-permitting studies, the density–latitude circulation of PERIANT8 displays an anticlockwise deep cell (here up to 20 Sv), a clockwise subpolar cell ( $\approx 5$  Sv), and an anticlockwise subtropical cell ( $\approx 15$  Sv) (see Döös and Webb 1994, for definitions of these cells). In addition, PERIANT8 displays a vigorous anticlockwise cell of 15 Sv in the lightest density ranges between  $65^\circ$  and  $45^\circ$ S.

The depth–latitude overturning (or Deacon Cell) has a maximum of 30 Sv (Fig. 2a). The total density–latitude overturning has a maximum of 5 Sv and a minimum of 15 Sv south of  $40^\circ$ S (Fig. 2a). So the combined

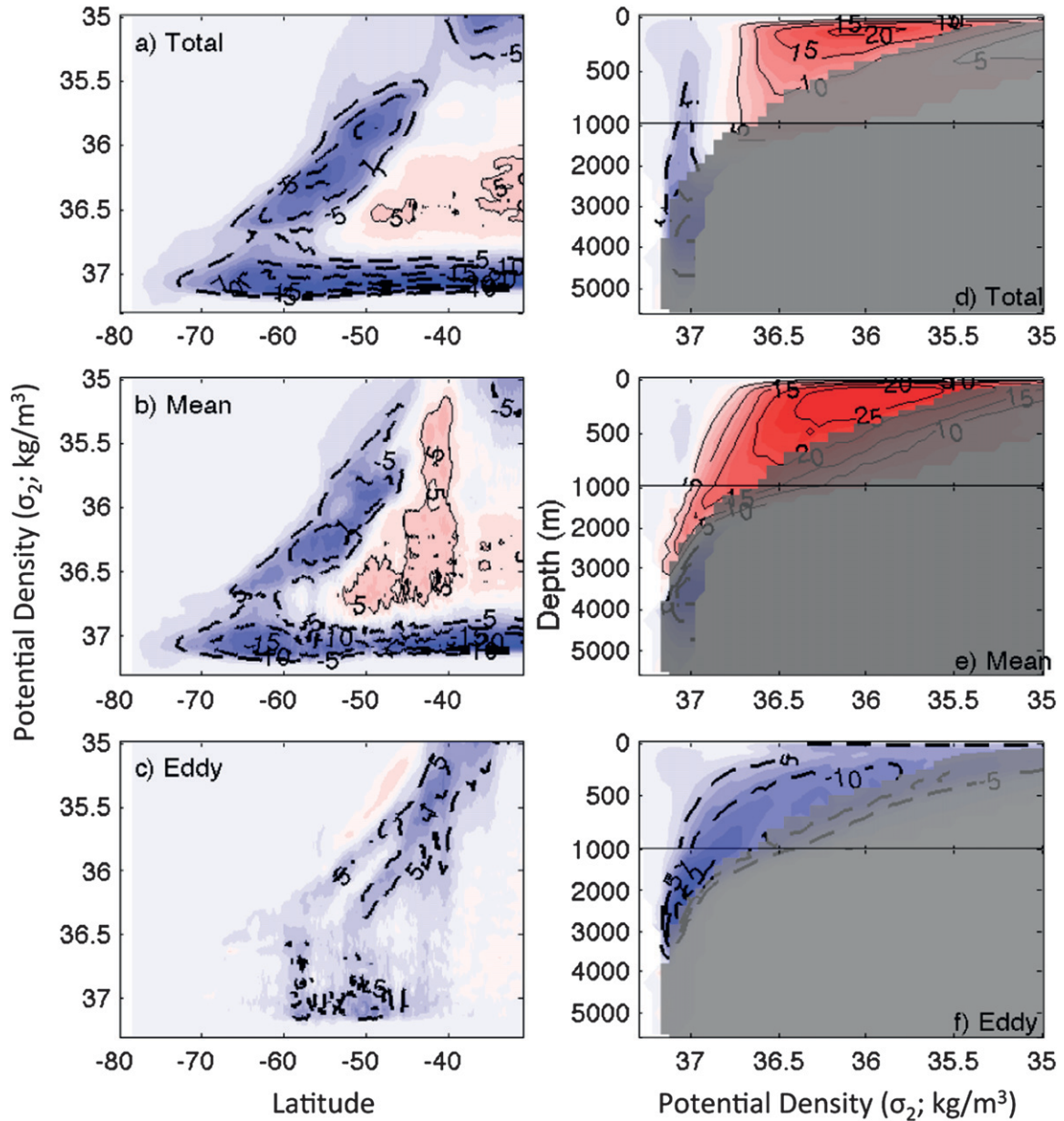


FIG. 3. (a) Overturning circulation of PERIANT8 averaged in density–latitude coordinates ( $\Psi_{y\sigma}$ ). (b) Eulerian mean contribution to circulation averaged in density–latitude coordinates ( $\bar{\Psi}_{y\sigma}$ ). (c) Transient contribution to the density–latitude circulation ( $\Psi'_{y\sigma}$ ). (d) Overturning circulation averaged in density–depth coordinates ( $\Psi_{\sigma z}$ ). (e) Eulerian mean contribution to circulation averaged in density–depth coordinates ( $\bar{\Psi}_{\sigma z}$ ). (f) Transient contribution to the circulation averaged in density–depth coordinates ( $\Psi'_{\sigma z}$ ). Positive cells are clockwise (solid contours) and negative cells are anticlockwise (dashed contours). In (d),(e),(f) shading shows depth–density ranges not wholly inside the model domain.

contribution to the density–latitude overturning due to standing meanders (any perturbation to the zonal mean) and transient eddies (any perturbation to the temporal mean) is 25–35 Sv. To determine to what degree standing meanders or transient eddies set the compensation of the Deacon Cell in density–latitude coordinates, we diagnose the Eulerian mean component  $\bar{\Psi}_{y\sigma}$  and transient component  $\Psi'_{y\sigma}$  of the overturning as

$$\bar{\Psi}_{y\sigma} = - \oint \int_{\sigma_2^* \leq \sigma_2} \bar{v}(x, y, z) dz dx, \quad \text{and} \quad (3)$$

$$\Psi'_{y\sigma} = \Psi_{y\sigma} - \bar{\Psi}_{y\sigma}. \quad (4)$$

Here,  $\bar{v}$  is the meridional velocity averaged in time on the model grid rather than at constant density

$\{\bar{v} = [1/(t_2 - t_1)] \int_{t_1}^{t_2} v dt\}$ . We use the general term *transient eddy* to describe the contribution due to all transient processes and do not distinguish between different temporal or spatial scales.

In PERIANT8, the Eulerian mean density–latitude overturning is similar in magnitude and spatial pattern to the total density–latitude overturning (Fig. 3b). The transient eddy overturning  $\Psi'_{y\sigma}$  only partially works against the Deacon Cell in PERIANT8 (Fig. 3c). Transient eddy overturning cells reach 10 Sv at a few latitudes and at scales of around 50 km. Averaged over the latitudes of Drake Passage, the transient eddy contribution to the density–latitude overturning is approximately 5 Sv. The Deacon cell is more strongly counteracted by standing meanders, which flux light water southward and dense water northward in response to the wind-driven Ekman and geostrophic transports, than by transient eddy fluxes.

To gain further insight into the Southern Ocean overturning, we average the overturning in depth–density coordinates (Nurser and Lee 2004; Nycander et al. 2007). Such a diagnostic represents the actual vertical transport of water masses and can be interpreted as the potential energy input into the ocean by the circulation at the reference pressure of the potential density coordinate (Nycander et al. 2007).

Killworth (1992) demonstrates that the ACC is close to equivalent barotropic, meaning the vertical shear is aligned with the flow direction. Via the thermal wind equation, contours of constant density and depth are perfectly aligned with the geostrophic shear. So, depth–density averaging has the additional advantage of being naturally “streamwise” along the ACC to the extent that it is equivalent barotropic.

Here we apply depth–density averaging in the Southern Ocean only. That is, only south of 30°S.

We define the depth–density streamfunction  $\Psi_{\sigma_z}$  as the integral of the vertical velocity  $w$  over the area of a constant depth surface where  $\sigma_2^* \geq \sigma_2$  such that

$$\Psi_{\sigma_z} = \frac{1}{t_2 - t_1} \int_{t_1}^{t_2} \int \int_{\sigma_2^* \geq \sigma_2} w(x, y, z, t) dx dy dt. \quad (5)$$

Above we apply a no-normal-flow condition at  $\sigma_2 = \infty$ , implying the integral must be from higher to lower density.

At any particular depth,  $\Psi_{\sigma_z}$  is the accumulated vertical transport in density coordinates (Fig. 4a). This interpretation holds, regardless of whether the model diagnosed is in a steady state or has open boundaries. If the model is in a steady state such that depth–density iso-volumes (i.e., those bound by surfaces of constant density and depth) have zero trend, such iso-volumes

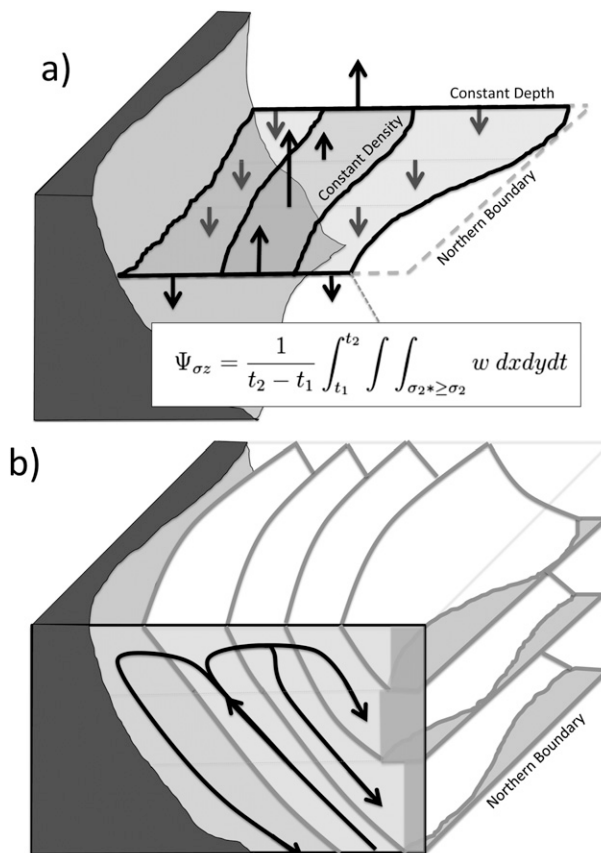


FIG. 4. Schematic describing how the depth–density streamfunction is computed. (a) Vertical velocity is summed at constant depth over areas bound by contours of constant density. (b) For density and depth ranges found wholly inside the domain of integration (here south of 30°S) the streamfunction represents the net pathway of water parcels in depth–density coordinates.

are contained wholly inside the model domain and there is a no-normal-flow condition linking  $\Psi_{\sigma_z}$  at different depths;  $\Psi_{\sigma_z}$  can be interpreted as the net pathway of water parcels in depth–density coordinates (Fig. 4b). If these conditions are met, the following also holds

$$\Psi_{\sigma_z}(z_1, \sigma_2) - \Psi_{\sigma_z}(z_0, \sigma_2) = \frac{1}{t_2 - t_1} \int_{t_1}^{t_2} \int \int_{z_0}^{z_1} w^{\sigma_2} dA dt. \quad (6)$$

Above,  $w^{\sigma_2}$  is the local diapycnal velocity across the  $\sigma_2$  surface. In our analysis, density–depth iso-volumes do exist at the northern boundary of the domain (at 30°S). So, the interpretation of  $\Psi_{\sigma_z}$  as the pathway of water masses can only hold at densities above the densest found at the northern boundary of the domain at a given depth. Densities that are found at the northern boundary of the domain (at any longitude or time) at a particular depth

are thus shaded in gray in all figures showing  $\Psi_{\sigma_2}$  (e.g., Figs. 3d,e,f).

As Nycander et al. (2007) point out, if the flow is steady, a depth–density overturning streamfunction describes a purely diabatic circulation. Vertical transports in density coordinates require exchanges of potential energy and diapycnal transports require net diapycnal mixing or deep sources of buoyancy. As we are using  $\sigma_2$  as our density variable this energetic interpretation holds at the 2000-m reference surface and in so far as pressure is a strong function of depth. (Alternative reference densities have been tested and the results presented here are qualitatively the same.)

Across the northern boundary of the PERIANT8 domain, volume fluxes can occur into depth–density isovolumes. These fluxes appear as source terms in any volume budget at constant density and depth. Figure 1a shows an example field of potential density at constant depth. Density ranges straddling the northern boundary are stippled in Fig. 1a. In diagnostics presented here, the depth–density streamfunction is shown for the entire domain and shading indicates depth–density ranges which straddle the northern boundary in Fig. 4b. Density–depth values that do not exist at all in the model are masked completely.

The total depth–density overturning  $\Psi_{\sigma_2}$  is computed from five-day averages of PERIANT8 (Fig. 3d). It reveals upwelling of circumpolar deep water between  $\sigma_2 = 36.5$  and  $37 \text{ kg m}^{-3}$ . Some of this deep water appears to remain at the surface and transform to lighter intermediate and mode waters and some appears to transform to denser AABW and sink back down below 2000-m depth. As we are integrating up to  $30^\circ\text{S}$  the accumulated streamfunction does not sum to zero as the transport is balanced at other latitudes.

In depth–density coordinates there is no anticlockwise surface cell in the upper layers. This indicates that the surface anticlockwise cell in density–latitude coordinates is, as Treguier et al. (2007) argue, an isobaric feature.

Other differences exist between the total density–latitude circulation and the depth–density overturning (Fig. 3a and Fig. 3d). The deep cell in density–latitude coordinates is more vigorous at up to 20 Sv while in depth–density coordinates less than 10 Sv is exchanged across the 2000-m-depth surface and less than 5 Sv across the 500-m-depth surface. This implies that, of the 20 Sv of bottom water that exits the Southern Ocean at  $40^\circ\text{S}$  (Fig. 3a), the majority of the volume transport balancing it enters at constant depth rather than actually upwelling to the Antarctic Shelf.

In the surface layers, the depth–density circulation displays a 15 Sv clockwise cell. Dense waters ( $\sigma_2 < 36.5 \text{ kg m}^{-3}$ ) to the south are upwelled through the

200-m-depth surface, while lighter water is downwelled ( $\sigma_2 < 36.5 \text{ kg m}^{-3}$ ) near the sea surface. This Deacon Cell–like feature does not exist in density–latitude coordinates.

As was done for the density–latitude streamfunction we separate the depth–density streamfunction into a mean and transient eddy component, such that

$$\bar{\Psi}_{\sigma_2} = \int \int_{\sigma_2^* \geq \bar{\sigma}_2} \bar{w}(x, y, z) dx dy, \quad \text{and} \quad (7)$$

$$\Psi'_{\sigma_2} = \Psi_{\sigma_2} - \bar{\Psi}_{\sigma_2}, \quad (8)$$

where  $\bar{\Psi}_{\sigma_2}$  is derived only from the Eulerian mean vertical velocity,  $[1/(t_2 - t_1) \int_{t_1}^{t_2} w dt]$ .

In depth–density coordinates the Eulerian mean circulation fluxes up to 25 Sv of dense water ( $\sigma_2 > 36.5 \text{ kg m}^{-3}$ ) upward and lighter water downward (Fig. 3e). In these coordinates, the transient circulation is greater than 10 Sv between 250- and 3000-m depth, peaking at 20 Sv at 2000-m depth. The transient eddy circulation acts to flux dense water downward and light water upward. In depth–density coordinates, the Eulerian mean flow is always clockwise and the transient eddy flow is always anticlockwise. The residual or total flow is roughly aligned with the slope of mean isopycnals in the interior, as in the conceptual framework of Marshall and Radko (2003). The difference in the standing meander and transient eddy contributions to the overturning in the two coordinates (Fig. 5) indicate that the two mechanisms contribute differently to the vertical and meridional exchanges of buoyancy.

We now wish to compare both the density–latitude and depth–density streamfunctions projected into geographical coordinates. Following Döös and Webb (1994), we project the density–latitude overturning into pseudodepth–latitude coordinates (Figs. 5a–c). The depth of isopycnals at each latitude is defined by the zonally averaged density (Fig. 2b), which is sorted to be monotonic with depth. (The average of  $z$  at constant  $\sigma_2$  would be more representative of the average depth of an isopycnal; however, as the highest densities occur at the surface, where they are formed, this approach would be less likely to be monotonic with depth.) As the densest waters in the Southern Ocean are formed at the Antarctic margins and the lightest tend to occur toward the equator, the depth–density overturning is projected into depth–pseudolatitude coordinates. Here, at constant depth, zonally averaged density is sorted to be monotonically decreasing with latitude. The streamfunction is then projected onto the latitude of each density (Figs. 5d,e). Note that when  $\Psi_{y\sigma}$  and  $\Psi_{\sigma_2}$  and their mean and transient components are computed no assumption of monotonicity with depth or latitude is used.

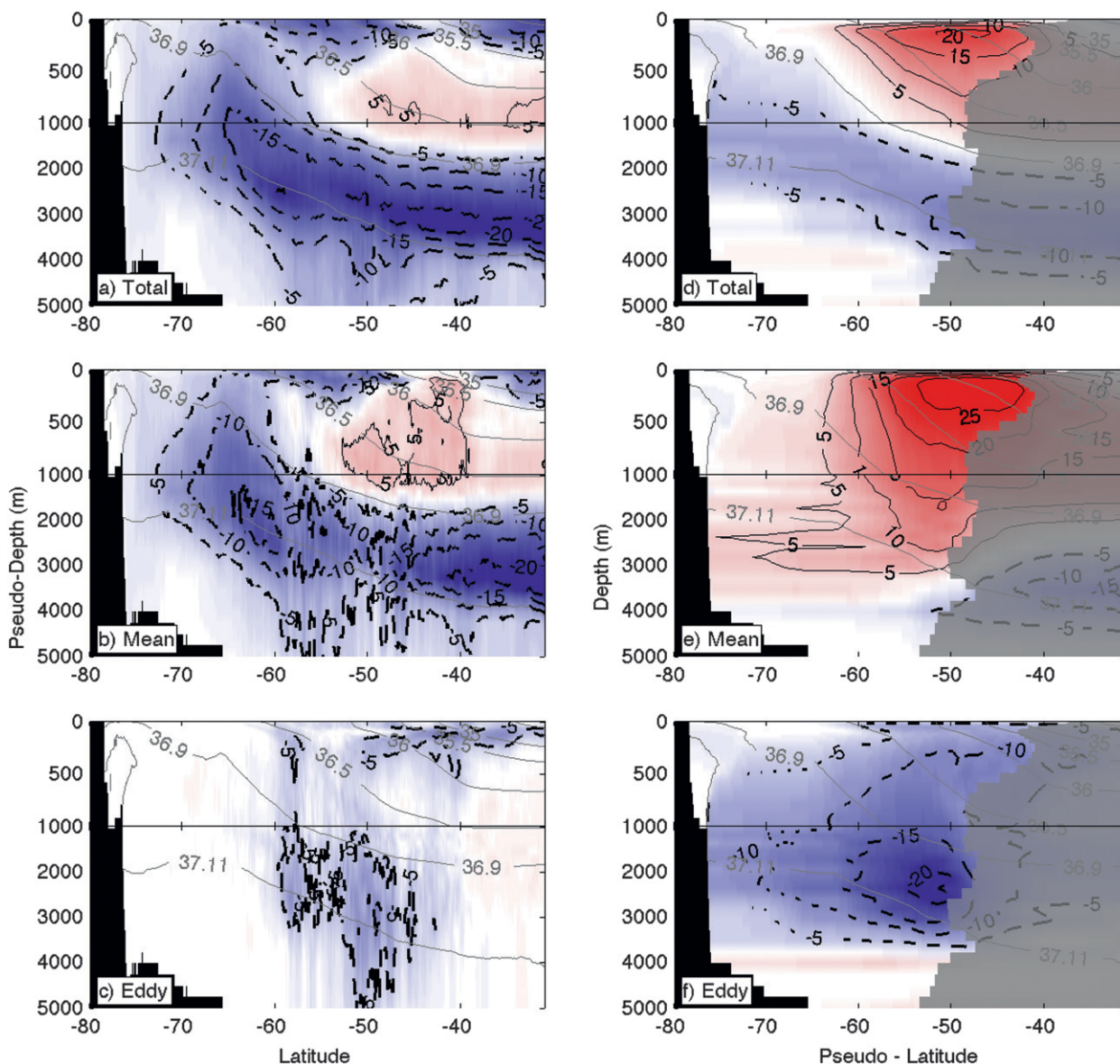


FIG. 5. (a)–(c) As in Figs. 3a–c, but projected from density–latitude coordinates into pseudodepth–latitude coordinates. (d)–(f) As in Figs. 3(d)–(f) but projected from depth–density coordinates into depth–pseudolatitude coordinates.

In Figs. 5d–f, as in Figs. 3d–f, density–depth values that have occurred at the northern boundary (at any longitude or time) are shaded in gray. This shading is done at the average latitude of the density–depth value in question. Again, this indicates regions where water can be exchanged at constant depth and density across the northern boundary, and thus the streamfunction cannot be interpreted as the net pathway of water masses.

The density–latitude circulation, projected into geographical coordinates (Fig. 5a), does not reveal an overturning consistent with the schematic representations of the Southern Ocean overturning of Speer et al.

(2000) who infer the overturning from buoyancy fluxes in density coordinates at the sea surface (i.e., using the framework first proposed by Walin 1982). The density–latitude overturning has a closed anticlockwise cell at the surface, fluxing light water southward and dense water northward, which is not seen in the framework of Speer et al. (2000) nor in model-based applications of such a method (Iudicone et al. 2008). In depth–density coordinates, however, circumpolar water masses upwell along isopycnals and are transformed at the surface into intermediate and bottom waters (Fig. 5d). The depth–density coordinates matches to the surface density framework used by Speer et al. (2000) as follows: 1) it

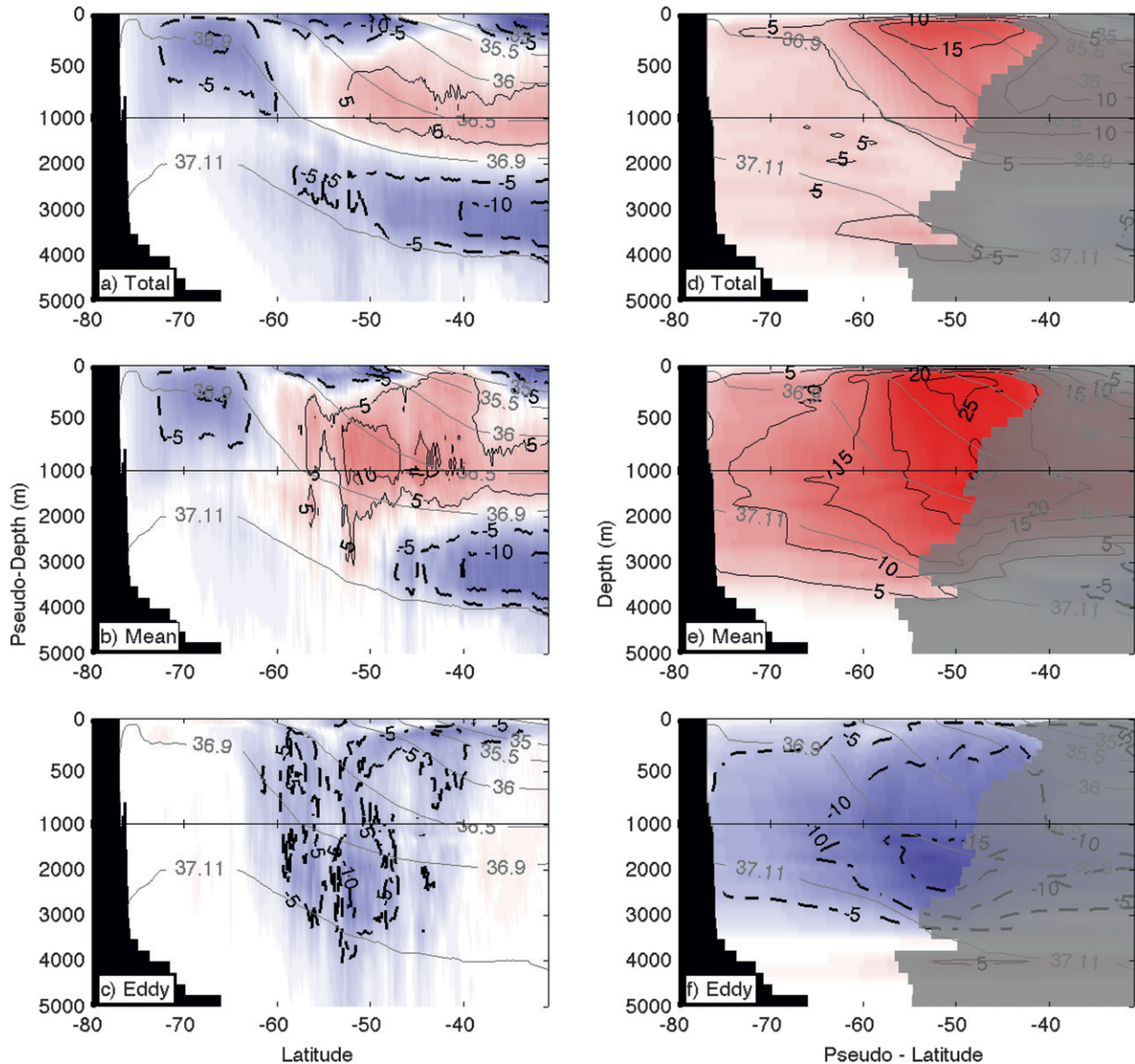


FIG. 6. As in Fig. 5, but for the simulation ORCA025. Density and depth ranges which straddle  $30^{\circ}\text{S}$  are shaded in gray in (d)–(f).

follows density contours at constant depth; and 2) it shows a net transformation of dense water into mode and intermediate waters.

### b. ORCA025 overturning

To complement our analysis of PERIANT8, we diagnose the density–latitude and depth–density circulation in the simulation ORCA025. As discussed in section 2, ORCA025 has a coarser resolution than PERIANT8 but, unlike PERIANT8, is a global model and has no bottom water restoring or open boundary. In addition, we are able to compare the depth–density approach to the density–streamline approach of Treguier et al.

(2007). For consistency, we compute overturning diagnostics in ORCA025 over the period 1991–2000 as in Treguier et al. (2007) made with the same ORCA025 model. Diagnostics in ORCA025 are computed only south of  $30^{\circ}\text{S}$  as in PERIANT8.

We diagnose the density–latitude streamfunction from five-day average output of ORCA025 (shown projected into pseudodepth–latitude coordinates; Figs. 6a–c). As Treguier et al. (2007) point out, there is a strong counterclockwise surface cell at latitudes of Drake Passage in the total density–latitude circulation. This cell is equivalent to that of PERIANT8 and in both models is mostly achieved by the Eulerian mean flow (Fig. 6b).

The bottom water cell in density–latitude coordinates is weaker in ORCA025 than in PERIANT8.

Again, the depth–density overturning is computed from five-day output of ORCA025 (shown projected into depth–pseudolatitude coordinates; Figs. 6d–f). As in PERIANT8, the total depth–density overturning appears to show upwelling along mean isopycnal surfaces. There is, however, no sinking of AABW in ORCA025. The bottom water cells seen in density–latitude coordinates may represent a circulation at constant depth where water enters from the north as lighter water and exits as denser water at the same depth. Transformations in the deep cell in ORCA025 either imply density being mixed down along the Antarctic Shelf rather than advected downward or that dense water is being advected out of the Southern Ocean and the model is still adjusting. Such adjustment is suggested also by the gradual decrease in ACC transport in ORCA025 throughout the ORCA025-G70 simulation (Treguier et al. 2010).

The density–depth overturning of ORCA025 (Fig. 6d) is always clockwise, fluxing dense water upward and lighter water downward, while the density–latitude circulation (Fig. 6a) has both clockwise and anticlockwise cells. This suggests that the anticlockwise surface cell and the AABW cell in density–latitude coordinates do not represent actual upwelling and downwelling of water masses in this model.

As in PERIANT8, the density–latitude circulation of ORCA025 is achieved largely through a balance between the zonally averaged wind-forced circulation (not shown but practically identical to Fig. 2a) and the standing transport that counteracts it. Transient eddy fluxes play a smaller role than standing meanders. However, in depth–density coordinates, transient eddy fluxes do play a major role in countering the wind-driven Eulerian mean circulation.

Treguier et al. (2007) take the novel approach of diagnosing the circulation of ORCA025 in density–mean streamline coordinates. This approach has the advantage of filtering out the “standing meander” transport. Comparing the depth–density overturning from ORCA025 (Figs. 6d–f) to the density–streamline analysis of (Treguier et al. 2007, see their Figs. 9, 10, and 11) we find that the two diagnostics are indeed equivalent. Both Treguier et al. (2007) and our study show a strong Eulerian mean overturning of up to 25 Sv, which is countered by a transient eddy cell of more than 15 Sv. The total circulation in both the depth–density analysis of this study and the density–streamline analysis of Treguier et al. (2007) is up to 10 Sv and closely follows isopycnal layers away from the sea surface.

### c. *PERIANT025 overturning with perturbed wind forcing*

We now analyze the last 10 years of simulations PERIANT025-REF and PERIANT025-SAM discussed in Dufour et al. (2012). PERIANT025-REF is a regional extraction of ORCA025. PERIANT025-REF has a density–latitude overturning circulation with surface and subpolar cells within 10%–20% of the magnitude of those in ORCA025 (see Fig. 6 of Dufour et al. (2012)). The deep cell of PERIANT025-REF is stronger, most likely because of the deep restoring of bottom waters.

To produce PERIANT025-SAM, Dufour et al. (2012) perturb the model with a wind field consistent with a fixed increase in the southern annular mode (SAM; Thompson and Wallace 2000) of two times its observed standard deviation for the 25-yr duration of the experiment. This increases the strength of the westerly wind stress by approximately 30% and shifts its peak to the south by 3° of latitude (Fig. 1b of Dufour et al. 2012). We diagnose the anomaly in both the density–latitude circulation for the SAM perturbation runs. We do this by subtracting the circulation for PERIANT025-REF from that of PERIANT025-SAM. The anomalous circulation and its Eulerian and transient components are shown in Figs. 7a–c.

As reported by Dufour et al. (2012), the total density latitude overturning shows an increase in the peak of the subpolar cell of approximately 3 Sv (Fig. 7a). The transient-eddy component of the density–latitude overturning in PERIANT025-SAM relative to PERIANT025-REF increases at some latitudes and decreases in others, despite the broad increase in wind stress. This is somewhat surprising, in the context of the present literature, as it is commonly assumed that, in density–depth coordinates, transient eddies will increase to counter changes in the wind-driven zonal-mean overturning (Meredith et al. 2012). Dufour et al. (2012) find that the increase in the wind-driven zonally averaged overturning with the SAM forcing is countered most strongly by a change in the meridional density–latitude circulation because of standing meanders, fluxing more light water southward and dense water northward. There are regions where the transient-eddy density–depth overturning does show a large change, with patches of  $-6$  Sv change the deep cell and  $+4$  Sv in the surface cell for example. These changes are large, but are difficult to relate directly to the forcing and are likely in response both to changes in the wind forcing and changes in the mean geostrophic flow.

In density–depth coordinates the circulation of PERIANT025-REF is also equivalent to that of ORCA025 to within 10%–20% (not shown), with the

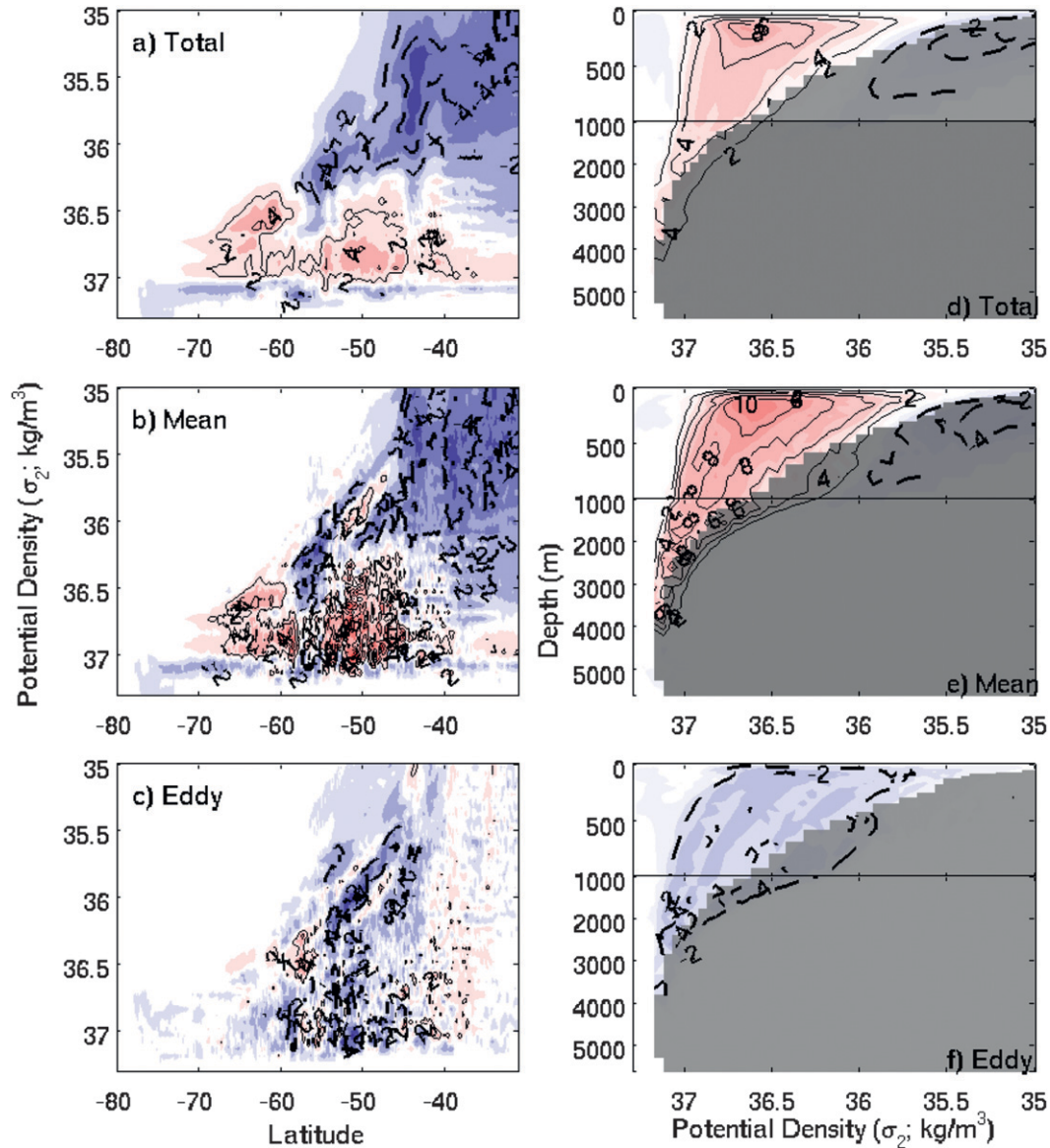


FIG. 7. As in Fig. 3, but for the difference between simulation PERIANT025-SAM and PERIANT025-REF. Contour intervals are 2 Sv rather than the 5 Sv in Fig. 3. Density and depth ranges which straddle 30°S in PERIANT025-SAM are shaded in gray.

exception the Antarctic Bottom Water cell, which does exist in PERIANT025-REF but is weak at less than 5 Sv. The density–depth overturning of PERIANT025-SAM minus that of PERIANT025-REF and its Eulerian and transient components are shown in Figs. 7d–f. The total overturning increases by up to 8 Sv near the surface and 4–5 Sv at 1000-m depth with the SAM forcing. The transient eddy overturning in depth–density coordinates increases with the SAM forcing by up to 4 Sv at 1000 m. As the winds act to flux more dense water upward to the south and flux more light water downward to the north, the transient eddy component of the circulation acts

against the wind, fluxing more dense water downward and light water upward.

#### 4. Discussion

We have diagnosed the depth–density overturning in both a simulation with sinking water around Antarctica (PERIANT8, albeit with deep restoring around Antarctica) and another with no sinking of bottom water at all (ORCA025). Unlike PERIANT8, there is very little sinking of dense water in PERIANT025-REF either (not shown). The result that fluxes because of transient

eddies are larger than those because of standing meanders in the vertical holds in both ORCA025, PERIANT8, and PERIANT025. This result cannot be confirmed, however, until a range of realistic eddying models that describe steady formation of bottom water exist. Challenges indeed remain in this regard (Lee et al. 2002; Treguier et al. 2007).

Like PERIANT8, PERIANT025 has deep restoring but still does not manage to create sinking of Antarctic bottom water (Fig. 7). An equivalent experiment at  $\frac{1}{2}^\circ$  resolution, PERIANT05, Dufour et al. (2012), also fails to produce sinking AABW, despite deep restoring (not shown). This suggests that it is either the change in freshwater forcing around Antarctica in PERIANT8 that permits the AABW cell or that the transition from  $\frac{1}{4}^\circ$  to  $\frac{1}{8}^\circ$  resolution represents a critical threshold in permitting the descent of AABW in this modeling framework.

Promisingly, the use of depth–density coordinates allows one to identify whether sinking of water masses is in fact occurring (as this is precisely what is being measured). Existing density–latitude and depth–latitude diagnostics can show a bottom water cell when no bottom water is actually sinking from the Antarctic Shelf (Fig. 6a).

Theoretical representations of the Southern Ocean describe a wind-forced circulation tilting isopycnals, transient-eddy fluxes acting to flatten these isopycnal slopes and a residual circulation related directly to buoyancy forcing at the surface and diapycnal mixing in the interior (Marshall and Radko 2003; Speer et al. 2000; Ito and Marshall 2008; Marshall 1997). Because of the presence of strong topographically steered meanders along the ACC, density–latitude diagnostics of eddy-permitting models do not reproduce these theoretical balances. In addition, transformations in density–latitude coordinates do not directly relate to constant latitude buoyancy fluxes as transformations can occur in the many density layers that outcrop in the Southern Ocean at a given latitude (Treguier et al. 2007).

In depth–density coordinates, there is a clear separation between flows near the surface, which are exposed to buoyancy forcing, and deep circulations whose diapycnal excursions, in steady state, can only occur because of mixing and nonlinear processes. In addition, the depth–density framework matches perfectly with the water mass transformation framework of Walin (1982) at the sea surface. In depth–density coordinates, the circulation has a direct link to energetics. If transient eddies always act to remove potential energy from the mean flow (i.e., are primarily driven by baroclinic instability) then eddy cells will always have one direction in these coordinates.

Here we have argued that depth–density coordinates are “naturally streamwise.” In an independent study to ours, Viebahn and Eden (2012) compute the overturning of a channel model in density–streamline coordinates with streamlines set by time mean density contours at constant depth. They find that the standing meander component of the overturning is minimized close to the chosen depth suggesting that density contours at constant depth are, indeed, a good proxy for local streamlines of the ACC.

McDougall (1987) argues that neutral density is the most appropriate density coordinate as water parcels can move adiabatically along neutral tangent planes without restoring buoyancy forces. As neutral density surfaces are tangent to locally referenced potential density surfaces, contours of constant neutral density and pressure follow contours of constant in situ density and pressure (locally referenced potential density is equivalent to in situ density at the reference depth). Thus pressure–in situ density coordinates (which are very close to a depth–in situ density coordinate in our simulations) is a “naturally neutral” coordinate. Here we have chosen to average in a depth–potential density coordinate so that a clear comparison is made with the potential density–latitude circulation. We advise that future studies, which are diagnosing a streamfunction at a particular level, diagnose the circulation in a pressure or depth–in situ density coordinate.

## 5. Conclusions

Multidecadal simulations performed with global and regional ocean models at  $\frac{1}{4}^\circ$  and  $\frac{1}{8}^\circ$  resolutions have been used to understand the dynamics of the Southern Ocean overturning and its response to forcing. We have calculated streamfunctions in both density–latitude and depth–density coordinates. By doing so we have elucidated the complementary roles of both standing meanders and transient eddies in the response to the wind forced Deacon Cell.

The density–latitude overturning  $\Psi_{y\sigma}$  shows how the Deacon Cell’s meridional exchanges are most strongly compensated by standing features of the circulation. The depth–density overturning  $\Psi_{\sigma z}$ , however, demonstrates how the upward transport of dense water and downward transports of light water by the Deacon Cell are compensated more strongly by transient eddy fluxes.

The schematic view of the overturning, according to Döös and Webb (1994), is one where water parcels follow the mean flow. The culmination of many standing meanders, each deviating by only a hundred meters or so in the vertical, leads, they argue, to cancel out the Deacon Cell. Here we find that standing meanders of the

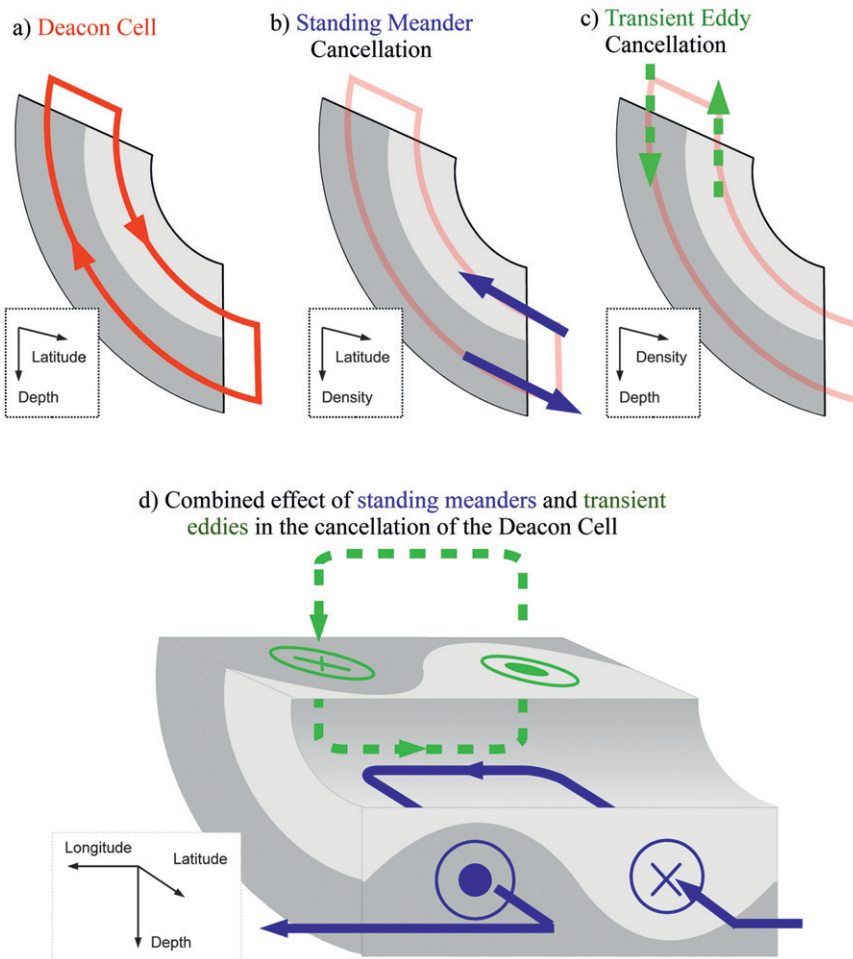


FIG. 8. Schematic diagram showing how the transient eddy overturning can play a major role in counteracting the wind-induced deacon cell vertically while playing a minor role meridionally and represents the extreme case scenario observed in the PERIANT025-SAM simulation. (a) Flow at constant latitude and depth reveals a closed “Deacon Cell” (red) transporting light water (light gray) downward and northward and dense water (dark gray) southward and upward. (b) Averaging at constant latitude and density shows a cancellation of the Deacon Cell by the mean flow (blue). (c) Averaging at constant depth and density shows a cancellation by transient eddy transport (green). (d) Standing meanders of the ACC transport light water southward through a cross section at constant latitude while transient eddies transport the same light water upward through a horizontal cross section. Together, the standing meanders and transient eddies, cancel the Deacon Cell.

ACC do compensate for the Deacon Cell most strongly in the meridional direction, but less so vertically. We find that transient eddies compensate less significantly for the Deacon Cell meridionally, but they do compensate significantly in the vertical.

An extreme example is presented in the perturbation simulation PERIANT025-SAM. In PERIANT025-SAM, westerly winds are increased. The winds drive light water northward and dense water southward. At the same time, standing meanders transport more light water southward and more dense water northward,

acting against changes in the wind driven circulation. At some latitudes, transient eddies transport no more dense water southward and light water northward than they did when winds were weaker. In contrast, as the wind increase, transient eddies do act to flux more dense water downward and light water upward, countering the wind-induced circulation. Although the true system is inevitably more complicated, Fig. 8 gives a schematic representation of how standing meanders can counter the wind-driven circulation in density–latitude coordinates, while simultaneously, transient

eddies counter the wind-driven circulation in density–depth coordinates.

Finally, transient eddies are found here to play a key role in the vertical exchange of water masses. It has been established previously that transient eddies play a minor role in meridional heat and freshwater transport in the Southern Ocean (Meijers et al. 2007). We propose a similar analysis to that carried out here, separating mean and transient components of vertical heat and freshwater transports, may reveal a key role for transient eddies.

*Acknowledgments.* We thank Rosemary Morrow, Francesco D’Ovidio for valuable contributions to this project, and George Nurser, John Marshall, and Alberto Naveira-Garabato for useful comments on this manuscript. We acknowledge the numerous interactions with members of the Drakkar consortium including the use of output from the ORCA025-G70 simulation. This work was partially funded by the ANR through Contract ANR-08-JCJC-0777-01. Support from CNRS/INSU through the LEFE Program (C02SUD project) is also acknowledged. Research leading to these results has received funding from the European Community’s Seventh Program FP7/2007-2013 under Grant agreement 283367 (MyOcean2). Simulations were performed at CINES (Montpellier, France) and IDRIS (Orsay, France).

#### REFERENCES

- Barnier, B., and Coauthors, 2006: Impact of partial steps and momentum advection schemes in a global ocean circulation model at eddy-permitting resolution. *Ocean Dyn.*, **300**, 543–567.
- Blanke, B., and P. Delecluse, 1993: Variability of the tropical Atlantic Ocean simulated by a general circulation model with two different mixed layers. *J. Phys. Oceanogr.*, **23**, 1363–1388.
- Brodeau, L., B. Barnier, T. Penduff, and A.-M. Treguier, 2010: An ERA-40 based atmospheric forcing for global ocean circulation models. *Ocean Modell.*, **31**, 88–104.
- Döös, K., and D. Webb, 1994: The Deacon cell and other meridional cells of the Southern Ocean. *J. Phys. Oceanogr.*, **24**, 429–442.
- Drakkar-Group, 2007: Eddy-permitting Ocean Circulation Hindcasts of past decades. *CLIVAR Exchanges*, Vol. 12, International CLIVAR Project Office, Southampton, United Kingdom, 8–10.
- Dufour, C. O., J. Le Sommer, J. D. Zika, M. Gehlen, J. C. Orr, P. Mathiot, and B. Barnier, 2012: Standing and transient eddies in the response of the Southern Ocean meridional overturning to the southern annular mode. *J. Climate*, **25**, 6958–6974.
- Hallberg, R. W., and A. Gnanadesikan, 2006: The role of eddies in determining the structure and response of the wind-driven Southern Hemisphere overturning: Results from the Modelling Eddies in the Southern Ocean (MESO) project. *J. Phys. Oceanogr.*, **36**, 2232–2251.
- Ito, T., and J. Marshall, 2008: Control of lower limb circulation in the Southern Ocean by diapycnal mixing and mesoscale eddy transfer. *J. Phys. Oceanogr.*, **38**, 2832–2845.
- Iudicone, D., G. Madec, and T. McDougall, 2008: Water-mass transformations in a neutral density framework and the key role of light penetration. *J. Phys. Oceanogr.*, **38**, 1357–1376.
- Killworth, P., 1992: An equivalent barotropic mode in the fine resolution Antarctic model. *J. Phys. Oceanogr.*, **22**, 1379–1387.
- Lee, M.-M., and A. C. Coward, 2003: Eddy mass transport for the southern ocean in an eddy-permitting global ocean model. *Ocean Modell.*, **5**, 249–266.
- , and A. J. G. Nurser, 2012: Eddy subduction and the vertical transport streamfunction. *J. Phys. Oceanogr.*, **42**, 1762–1780.
- , A. C. Coward, and A. J. G. Nurser, 2002: Spurious diapycnal mixing of the deep waters in an eddy-permitting global ocean model. *J. Phys. Oceanogr.*, **32**, 1522–1535.
- Madec, G., 2008: NEMO ocean engine. IPSL Note du Pôle de Modelisation 27, 209 pp.
- Manabe, S., K. Bryan, and M. J. Spelman, 1990: Transient response of a global ocean–atmosphere model to a doubling of atmospheric carbon dioxide. *J. Phys. Oceanogr.*, **20**, 722–749.
- Marshall, D., 1997: Subduction of water masses in and eddying ocean. *J. Mar. Res.*, **55**, 201–222.
- Marshall, J., and T. Radko, 2003: Residual-mean solutions for the Antarctic Circumpolar Current and its associated overturning circulation. *J. Phys. Oceanogr.*, **33**, 2341–2354.
- McDougall, T. J., 1987: Neutral surfaces. *J. Phys. Oceanogr.*, **17**, 1950–1964.
- Meijers, A. J., N. L. Bindoff, and J. L. Roberts, 2007: On the total, mean, and eddy heat and freshwater transports in the Southern Hemisphere of a 1/8° by 1/8° global ocean model. *J. Phys. Oceanogr.*, **37**, 277–295.
- Meredith, M. P., A. C. Naveira-Garabato, A. M. Hogg, and R. Farneti, 2012: Sensitivity of the overturning circulation in the Southern Ocean to decadal changes in wind forcing. *J. Climate*, **25**, 99–100.
- Nurser, A. J. G., and M.-M. Lee, 2004: Isopycnal averaging at constant height. Part I: The formulation and a case study. *J. Phys. Oceanogr.*, **34**, 2721–2739.
- Nycander, J., J. Nilsson, K. Döös, and G. Bromström, 2007: Thermodynamic analysis of ocean circulation. *J. Phys. Oceanogr.*, **37**, 2038–2052.
- Penduff, T., M. Juza, L. Brodeau, G. C. Smith, B. Barnier, J.-M. Molines, A.-M. Treguier, and G. Madec, 2010: Impact of global ocean model resolution on sea level variability with emphasis on interannual time scales. *Ocean Sci.*, **6**, 269–284.
- Polton, J. A., and D. P. Marshall, 2007: Overturning cells in the Southern Ocean and subtropical gyres. *Ocean Sci.*, **3**, 17–30.
- Rintoul, S. R., C. Hughes, and D. Olbers, 2001: The Antarctic circumpolar current system. *Ocean Circulation and Climate*, G. Siedler, J. Church, and J. Gould, Eds., Academic Press, 271–302.
- Sabine, C. L., and Coauthors, 2004: The oceanic sink for anthropogenic CO<sub>2</sub>. *Science*, **305**, 367–371.
- Speer, K. G., S. R. Rintoul, and B. M. Sloyan, 2000: The diabatic Deacon cell. *J. Phys. Oceanogr.*, **30**, 3212–3222.
- Thompson, D. W. J., and J. M. Wallace, 2000: Annular modes in the extratropical circulation. Part I: Month-to-month variability. *J. Climate*, **13**, 1000–1016.

- Treguier, A. M., B. Barnier, A. de Miranda, J.-M. Molines, N. Grima, M. Imbard, and G. Madec, 2001: An eddy permitting model of the atlantic circulation: evaluating open boundary conditions. *J. Geophys. Res.*, **106** (C10), 22 115–22 129.
- , M. England, S. Rintoul, G. Madec, J. Le Sommer, and J. M. Molines, 2007: Southern Ocean overturning across streamlines in an eddy simulation of the Antarctic Circumpolar Current. *Ocean Sci.*, **3**, 491–507.
- , J. Le Sommer, J. M. Molines, and B. de Cuevas, 2010: Response of the Southern Ocean to the southern annular mode: Interannual variability and multidecadal trend. *J. Phys. Oceanogr.*, **40**, 1659–1668.
- Viebahn, J., and C. Eden, 2012: Standing eddies in the meridional overturning circulation. *J. Phys. Oceanogr.*, **42**, 1486–1508.
- Walín, G., 1982: On the relation between sea–surface heat flow and thermal circulation in the ocean. *Tellus*, **34**, 187–195.